A Generalized Space-Mapping Tableau Approach to Device Modeling

John W. Bandler, *Fellow, IEEE*, Natalia Georgieva, *Member, IEEE*, Mostafa A. Ismail, *Student Member, IEEE*, José E. Rayas-Sánchez, *Senior Member, IEEE*, and Qi-Jun Zhang, *Senior Member, IEEE*

***Abstract*—A comprehensive framework to engineering device modeling, which we call generalized space mapping (GSM) is introduced in this paper. GSM permits many different practical implementations. As a result, the accuracy of available empirical models of microwave devices can be significantly enhanced. We present three fundamental illustrations: a basic space-mapping super model (SMSM), frequency-space-mapping super model (FSMSM) and multiple space mapping (MSM). Two variations of MSM are presented: MSM for device responses and MSM for frequency intervals. We also present novel criteria to discriminate between coarse models of the same device. The SMSM, FSMSM, and MSM concepts have been verified on several modeling problems, typically utilizing a few relevant full-wave electromagnetic simulations. This paper presents four examples: a microstrip line, a microstrip right-angle bend, a microstrip step junction, and a microstrip shaped T-junction, yielding remarkable improvement within regions of interest.**

***Index Terms*—Empirical models, frequency mapping, modeling, passive devices, space mapping.**

I. Introduction

WE GENERALIZE the space mapping (SM) [1], the frequency space mapping (FSM) [2] and the multiple space mapping (MSM) [3] concepts to build a new engineering device modeling framework. This framework is flexible enough to permit a number of implementable special cases. The important observation that we make is that the methodology closely follows sound engineering design practice. Our contribution is a mathematical formulation suitable for device modeling and a clear practical interpretation. We refer to the concept generically as the generalized space-mapping (GSM) concept.

The mathematical formulation of the GSM framework is not complicated. It is expected to be useful in assisting designers to evaluate the accuracy of empirical models and/or to discriminate between them. Intuitively meaningful quantitative measures of model accuracy can be developed through careful interpretations of GSM.

Significant enhancement of the accuracy of available empirical models of microwave devices can be realized. Three fundamental cases are presented: space-mapping super model (SMSM), which maps designable device parameters, a basic frequency-space mapping super model (FSMSM), which maps the frequency variable as well as the designable device parameters and MSM. We present two variations of MSM: multiple space mapping for device responses (MSMDR) and multiple space mapping for frequency intervals (MSMFI). In MSMDR, we divide the set of device responses into a number of sub-responses and establish a separate mapping for each sub-response. In MSMFI, we divide the frequency range of interest into a number of intervals and establish a separate mapping for each interval. Two algorithms to implement MSMDR and MSMFI are also presented.

Two model types are usually defined in the SM process [1]: a "coarse" model, typically an empirical model, and a "fine" model, typically a full-wave electromagnetic (EM) simulator. Empirical models of microwave devices behave well in certain parameter and frequency regions. They are computationally very fast and are preferred for initial design purposes over accurate, but CPU intensive full-wave EM simulators.

The basic SMSM, FSMSM, and MSM concepts have been validated on a number of modeling problems, typically utilizing a few relevant full-wave EM simulations. This paper presents four illustrations: a microstrip line, microstrip right-angle bend, microstrip step junction, and a microstrip-shaped T-junction, yielding remarkable improvement within the regions of interest.

II. GSM Concept

Consider a microwave device with physical parameters represented by an n-dimensional vector $\boldsymbol{x}_f$. In general, the response $\boldsymbol{R}_c(\boldsymbol{x}_f, \omega)$ produced by the coarse model deviates from the response $\boldsymbol{R}_f(\boldsymbol{x}_f, \omega)$ produced by an EM simulator, where ω is the frequency variable. Therefore, the aim is to find a mapping from the fine-model parameters and the frequency variable to a new set of parameters and a new frequency variable so that the responses of the two models match. Mapping the space parameters was introduced by Bandler *et al.* [1] and mapping the frequency variable was introduced later in [2]. The mapped coarse-model parameters are represented by an n-dimensional vector $\boldsymbol{x}_c$ and the mapped frequency variable is represented by ω_c. We call

Manuscript received June 16, 1999. This work was supported in part by the Natural Sciences and Engineering Research Council of Canada under Grant OGP0007239 and Grant STP0201832, by Com Dev, and by the Micronet Network of Centres of Excellence. The work of J. E. Rayas-Sánchez was supported by the Consejo Nacional de Ciencia y Tecnología, Mexico, and by the Instituto Tecnológico y de Estudios Superiores de Occidente, Mexico. The work of N. Georgieva was supported by the Natural Sciences and Engineering Research Council of Canada under a Post-Doctorate Fellowship.

J. W. Bandler is with the Simulation Optimization Systems Research Laboratory and the Department of Electrical and Computer Engineering, McMaster University, Hamilton, ON, Canada L8S 4K1 and is also with the Bandler Corporation, Dundas, ON, Canada L9H 5E7.

N. Georgieva, M. A. Ismail, and J. E. Rayas-Sánchez are with the Simulation Optimization Systems Research Laboratory and the Department of Electrical and Computer Engineering, McMaster University, Hamilton, ON, Canada L8S 4K1.

Q.-J. Zhang is with the Department of Electronics, Carleton University, Ottawa, ON, Canada K1S 5B6.

Publisher Item Identifier S 0018-9480(01)00011-4.

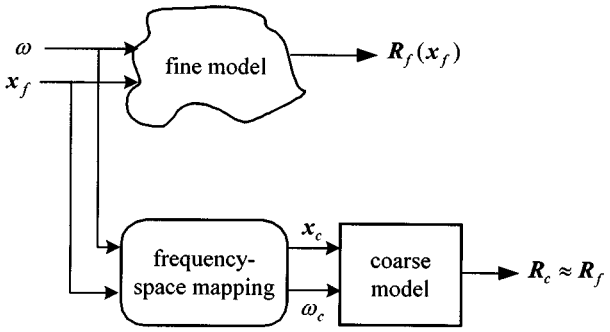

Fig. 1. FSMSM concept.

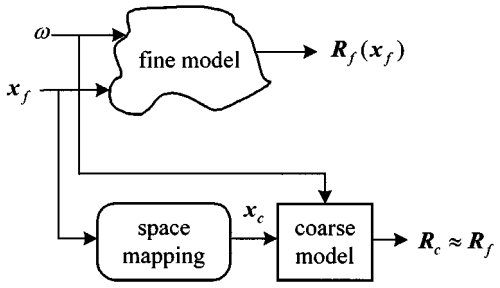

Fig. 2. SMSM concept.

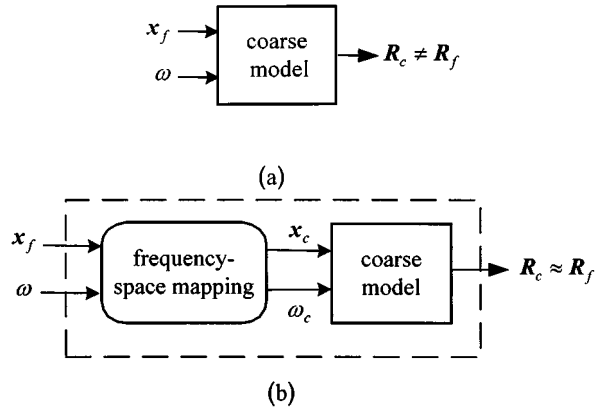

Fig. 3. (a) Coarse model. (b) Enhanced coarse model.

this scheme FSMSM, as illustrated in Fig. 1. A special case of FSMSM is to map only the fine-model parameters and leave the frequency variable unchanged. We call this the SMSM, as illustrated in Fig. 2. Once FSMSM or SMSM are established, the enhanced coarse model (see Fig. 3) can be utilized for analysis or design purposes. We will compare the FSMSM and SMSM in one of the examples.

The mapping relating the fine-model parameters and frequency to the coarse-model parameters and frequency is given by

$$[\boldsymbol{x}_c^T \quad \omega_c]^T = \boldsymbol{P}(\boldsymbol{x}_f, \omega). \tag{1}$$

Or, in matrix form, assuming a linear mapping

$$\begin{bmatrix} \boldsymbol{x}_c \\ \omega_c^{-1} \end{bmatrix} = \begin{bmatrix} \boldsymbol{c} \\ \delta \end{bmatrix} + \begin{bmatrix} \boldsymbol{B} & \boldsymbol{s} \\ \boldsymbol{t}^T & \sigma \end{bmatrix} \begin{bmatrix} \boldsymbol{x}_f \\ \omega^{-1} \end{bmatrix} \tag{2}$$

where $\{\boldsymbol{c}, \boldsymbol{B}, \boldsymbol{s}, \delta, \boldsymbol{t}, \sigma\}$ are the parameters characterizing the mapping $\boldsymbol{P}$. The constant vectors $\boldsymbol{c}$, $\boldsymbol{s}$, $\boldsymbol{t}$ are n-dimensional, $\boldsymbol{B}$ is an $n \times n$ matrix, and δ, σ are scalar. In (2), we notice that we map the inverse of the frequency (which is proportional to the wavelength) instead of the frequency itself. This has produced better results in all the models we considered than mapping the frequency directly. It can be also justified by the fact that, in most microwave structures, shrinking the structure would lead to a shift of its spectral characteristics to higher frequencies (shorter wavelengths).

The mapping parameters in (2) can be evaluated by solving the optimization problem

$$\min_{\boldsymbol{c}, \boldsymbol{B}, \boldsymbol{s}, \delta, \boldsymbol{t}, \sigma} \left\| [\boldsymbol{e}_1^T \quad \boldsymbol{e}_2^T \quad \cdots \quad \boldsymbol{e}_N^T]^T \right\| \tag{3}$$

subject to suitable constraints, where $\| \|$ is a suitable norm, N is the total number of fine-model simulations, and $\boldsymbol{e}_k$ is an error vector given by

$$\boldsymbol{e}_k = \boldsymbol{R}_f(\boldsymbol{x}_{f_i}, \omega_j) - \boldsymbol{R}_c(\boldsymbol{x}_c, \omega_c) \tag{4a}$$

$$[\boldsymbol{x}_c^T \quad \omega_c]^T = \boldsymbol{P}(\boldsymbol{x}_{f_i}, \omega_j) \tag{4b}$$

with

$$i = 1, \ldots, B_p \tag{5a}$$

$$j = 1, \ldots, F_p \tag{5b}$$

$$k = j + (i-1)F_p \tag{5c}$$

where B_p is the number of base points and F_p is the number of frequency points per frequency sweep. The total number of fine-model simulations is $N = B_p F_p$. The constraints we impose on the mapping parameters are that the mapping parameters should be as close as possible to the parameters corresponding to a unit mapping $\boldsymbol{x}_c = \boldsymbol{x}_f$ and $\omega_c = \omega$, which corresponds to $\{\boldsymbol{c} = \boldsymbol{0}, \boldsymbol{B} = \boldsymbol{I}, \boldsymbol{s} = \boldsymbol{0}, \delta = 0, \boldsymbol{t} = \boldsymbol{0}, \sigma = 1\}$. These constraints are justified by the fact that the coarse model carries considerable physical characteristics of the fine model. Therefore, the optimum values of the mapping parameters should not severely deviate from the values corresponding to a unit mapping. To include these constraints, the objective function in (3) is modified as follows:

$$\min_{\boldsymbol{c}, \boldsymbol{B}, \boldsymbol{s}, \delta, \boldsymbol{t}, \sigma} \left\| \left[\boldsymbol{e}_1^T \ \boldsymbol{e}_2^T \ \cdots \ \boldsymbol{e}_N^T \ \boldsymbol{c}^T \ \boldsymbol{s}^T \ \boldsymbol{t}^T \ \Delta\boldsymbol{b}_1^T \ \Delta\boldsymbol{b}_2^T \ \cdots \ \Delta\boldsymbol{b}_n^T \ \Delta\sigma \ \delta \right]^T \right\| \tag{6}$$

where the error vectors $\boldsymbol{e}_1, \boldsymbol{e}_2, \ldots, \boldsymbol{e}_N$ are defined by (4a), the vectors $\Delta\boldsymbol{b}_1, \Delta\boldsymbol{b}_2, \ldots, \Delta\boldsymbol{b}_n$ are the columns of the matrix $\Delta\boldsymbol{B}$ given by

$$\Delta\boldsymbol{B} = \boldsymbol{B} - \boldsymbol{I} \tag{7}$$

and $\Delta\sigma$ is defined by

$$\Delta\sigma = \sigma - 1. \tag{8}$$

The numerical values of the mapping parameters in (2) can give the designer physically based intuitive information on the entire modeling process. The deviation of the optimal values of these parameters from those corresponding to a unit mapping

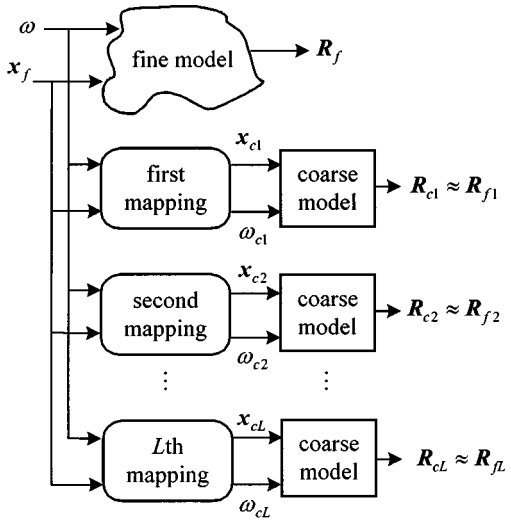

Fig. 4. MSMDR.

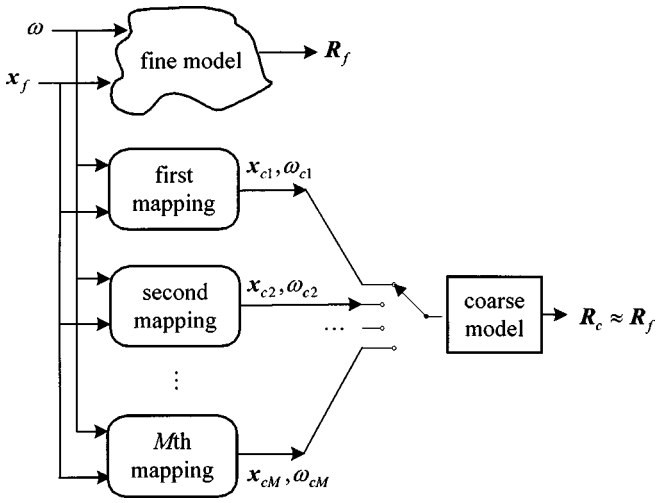

Fig. 5. MSMFI.

indicates the degree of proximity between the coarse and fine models. This important feature can be used to compare between two coarse models. The coarse model with less deviation should be more accurate. Let β be the deviation of the mapping parameters from the parameters corresponding to a unit mapping, i.e.,

$$\beta = \left\| [\boldsymbol{c}^T \quad \boldsymbol{s}^T \quad \boldsymbol{t}^T \quad \Delta\boldsymbol{b}_1^T \quad \Delta\boldsymbol{b}_2^T \quad \cdots \quad \Delta\,\boldsymbol{b}_n^T \quad \Delta\sigma\ \delta\,]^T \right\| \tag{9}$$

where $\Delta\boldsymbol{b}_1, \Delta\boldsymbol{b}_2, \ldots, \Delta\boldsymbol{b}_n$ and $\Delta\sigma$ are defined by (7) and (8), respectively. Therefore, based on the value of β, we can discriminate between various coarse models of the same device. The smaller the value of β, the closer the coarse model is to the fine model. We will demonstrate this feature in one of the examples.

III. MSM

MSM was introduced in [3]. We present two variations of MSM for device modeling. We refer to them as MSMDR and MSMFI. In MSMDR, we divide the device response vector $\boldsymbol{R}$ (in both models) into L subsets of responses (or vectors) $\boldsymbol{R}_i$, $i = 1, 2, \ldots, L$. An individual mapping is established for each subset of responses, as illustrated in Fig. 4. In MSMFI, we divide the frequency range of interest into M intervals and evaluate a separate mapping for each interval, as illustrated in Fig. 5 (the switch in Fig. 5 is controlled by the frequency variable). The important questions are how we divide these responses into a set of sub-responses and how we divide the frequency range into a set of intervals. There was no guide in [3] regarding the answer to these questions. The following algorithms implement MSMDR and MSMFI.

A. MSMDR Algorithm

The MSMDR algorithm divides the device responses in an iterative manner while establishing a separate mapping for each set of sub-responses. First, it establishes a mapping targeting all responses. It then assigns this mapping to the set of sub-responses satisfying a specified accuracy. It repeats the previous steps recursively on the remaining responses (which do not satisfy the required accuracy). The algorithm stops when all responses are exhausted. The following steps summarize the algorithm implementing MSMDR.

Step 1) Initialize $i = 1$ and let $\boldsymbol{R}$ contain all responses.
Step 2) Establish a mapping $\boldsymbol{P}_i$, by solving (6), targeting all responses in $\boldsymbol{R}$.
Step 3) Assign the mapping $\boldsymbol{P}_i$ to the set of sub-responses $\boldsymbol{R}_i \subset \boldsymbol{R}$ that satisfies the error criteria $\|\boldsymbol{R}_{f_i} - \boldsymbol{R}_{c_i}\| \leq \varepsilon$, where ε is a small positive number and $\boldsymbol{R}_{f_i}$, $\boldsymbol{R}_{c_i}$ are the fine and the coarse model sub-responses, respectively.
Step 4) Replace by $\boldsymbol{R}\boldsymbol{R} - \boldsymbol{R}_i$ and increment i.
Step 5) If $\boldsymbol{R}$ is not empty go to Step 2), otherwise stop.

We have to emphasize that MSMDR needs the same number of fine-model simulations (EM simulations) required to establish a single mapping targeting all responses. However, it can dramatically improve the coarse models, as we will see in the examples.

B. MSMFI Algorithm

The MSMFI algorithm is similar to the MSMDR algorithm. First, it establishes a mapping targeting all responses $\boldsymbol{R}$ in the whole frequency range $\omega_{\min} \leq \omega \leq \omega_{\max}$. It then assigns this mapping to the frequency interval $\omega_{\min} \leq \omega \leq \omega_1$ (where ω_1 belongs to the frequency range of interest) in which the set of responses $\boldsymbol{R}$ satisfies a certain specified accuracy. It repeats the previous steps recursively until covering the whole frequency range. The following steps summarize the MSMFI algorithm.

Step 1) Initialize $i = 1$ and let the frequency interval $\Omega = [\omega_{\min}, \omega_{\max}]$.
Step 2) Establish a mapping $\boldsymbol{P}_i$, by solving (6), in the frequency range defined by Ω.
Step 3) Assign the mapping $\boldsymbol{P}_i$ to the frequency interval $\Omega_i \subset \Omega$ in which the error criteria $\|\boldsymbol{R}_f - \boldsymbol{R}_c\| \leq \varepsilon$ is satisfied, where ε is a small positive number

and $\boldsymbol{R}_f$, $\boldsymbol{R}_c$ are the fine- and the coarse-model responses, respectively.

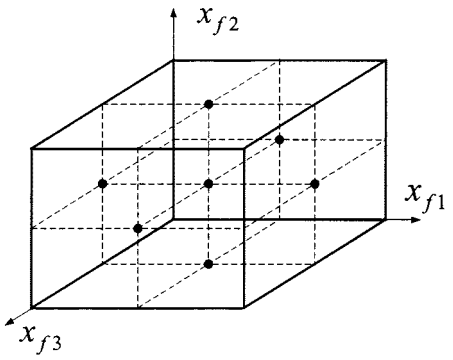

Fig. 6. Distribution of the base points in the region of interest for a three-dimensional space [5].

Step 4) Replace Ω by $\Omega - \Omega_i$ and increment i.

Step 5) If Ω is not empty go to Step 2), otherwise stop.

We have to emphasize that MSMFI costs the same number of fine-model simulations (EM simulations) required to establish a single mapping for the whole frequency range.

IV. Implementation of GSM

The optimization problem in (6) is solved using the Huber optimizer [4] implemented in OSA90/hope.[1] The norm used in (6) is also a Huber norm [4]. The Huber norm of an error vector $\boldsymbol{e} = [e_1 \;\; e_2 \;\; \ldots \;\; e_l]^T$ is defined by [4]

$$H(\boldsymbol{e}) = \sum_{i=1}^{l} \rho(e_i) \tag{10}$$

where

$$\rho(e_i) = \begin{cases} e_i^2/2, & \text{if } |e_i| \le \alpha \\ \alpha|e_i| - \alpha^2/2, & \text{if } |e_i| > \alpha \end{cases} \tag{11}$$

where α is a positive constant. The objective function in (6) is the Huber norm of the vector $\boldsymbol{e}$ given by

$$\boldsymbol{e} = \Big[\boldsymbol{e}_1^T \;\; \boldsymbol{e}_2^T \;\; \cdots \;\; \boldsymbol{e}_N^T \;\; \boldsymbol{c}^T \;\; \boldsymbol{s}^T \;\; \boldsymbol{t}^T \;\; \Delta\boldsymbol{b}_1^T \;\; \Delta\boldsymbol{b}_2^T \;\; \cdots \;\; \Delta\boldsymbol{b}_n^T \;\; \Delta\sigma \;\; \delta\Big]^T. \tag{12}$$

The Huber norm is robust against large errors and flexible with respect to small variations in the data [4]. The set of base points $\{\boldsymbol{x}_{f_i}, i = 1, 2, \ldots, B_p\}$ in the region of interest is taken as in [5] (see Fig. 6). According to this distribution, the number of base points is $2n + 1$, where n is the number of fine-model parameters. The starting values for the mapping parameters $\{\boldsymbol{c}, \boldsymbol{B}, \boldsymbol{s}, \delta, \boldsymbol{t}, \sigma\}$ are $\{\boldsymbol{0}, \boldsymbol{I}, \boldsymbol{0}, 0, \boldsymbol{0}, 1\}$, which correspond to the unit mapping $\boldsymbol{x}_c = \boldsymbol{x}_f$ and $\omega_c = \omega$. The software tools needed for the implementation of GSM are an optimizer (a Huber optimizer [4] is recommended), a suitable circuit simulator which can handle simple matrix operations, and a suitable full-wave EM simulator.

[1]OSA90/hope, version 4.0, Agilent EEsof EDA (formerly Optimization Systems Associates Inc.), Santa Rosa, CA 1997.

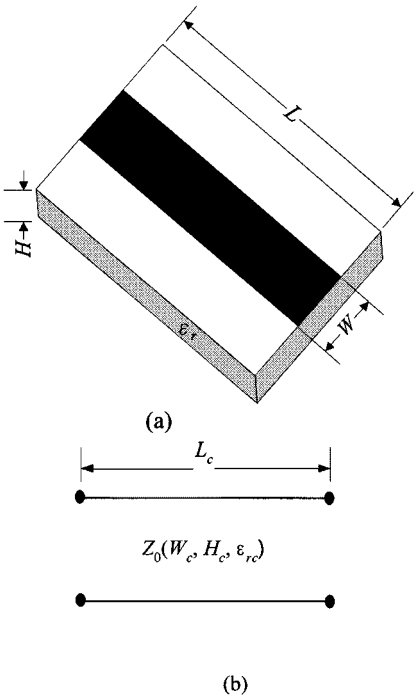

Fig. 7. Microstrip line models. (a) Fine model. (b) Coarse model.

V. Examples

We present four typical modeling problems: a microstrip line, microstrip right-angle bend, microstrip step junction, and microstrip-shaped T-junction. To display the results in a compact way, we define the error E_{ij} as the modulus of the difference between the scattering parameter S_{ij}^f computed by the fine model and the scattering parameter S_{ij}^c computed by the coarse model

$$E_{ij} = \left|S_{ij}^f - S_{ij}^c\right| = \sqrt{\left(\mathrm{Re}\left[S_{ij}^f\right] - \mathrm{Re}\left[S_{ij}^c\right]\right)^2 + \left(\mathrm{Im}\left[S_{ij}^f\right] - \mathrm{Im}\left[S_{ij}^c\right]\right)^2} \tag{13}$$

where $i = 1, 2, \ldots, M$ and $j = 1, 2, \ldots, M$ (M is the number of ports of the microwave device). The error E_{ij} is a measure of both the error in the magnitude and the phase of the scattering parameters S_{ij}^c. We refer to E_{ij} simply as the error in the scattering parameter S_{ij}.

A. Microstrip Line

In this example, we compare between SMSM and FSMSM. Both modeling approaches are used to enhance the transmission-line model of a microstrip line. The fine model is analyzed by Sonnet Software's *em* simulator[2] and the coarse model is a built-in element of OSA90/hope. The fine and coarse models are shown in Fig. 7. The structure in Fig. 7(a) was parameterized using Geometry Capture [6] implemented in Empipe.[3] The fine- and coarse-model parameters are given by $\boldsymbol{x}_f = [L \;\; W \;\; H \;\; \varepsilon_r]^T$, $\boldsymbol{x}_c = [L_c \;\; W_c \;\; H_c \;\; \varepsilon_{rc}]^T$. The region of interest is given

[2]*em*, version 4.0b, Sonnet Software Inc., Liverpool, NY 1998.

[3]Empipe, version 4.0, Agilent EEsof EDA (formerly Optimization Systems Associates Inc.), Santa Rosa, CA 1997.

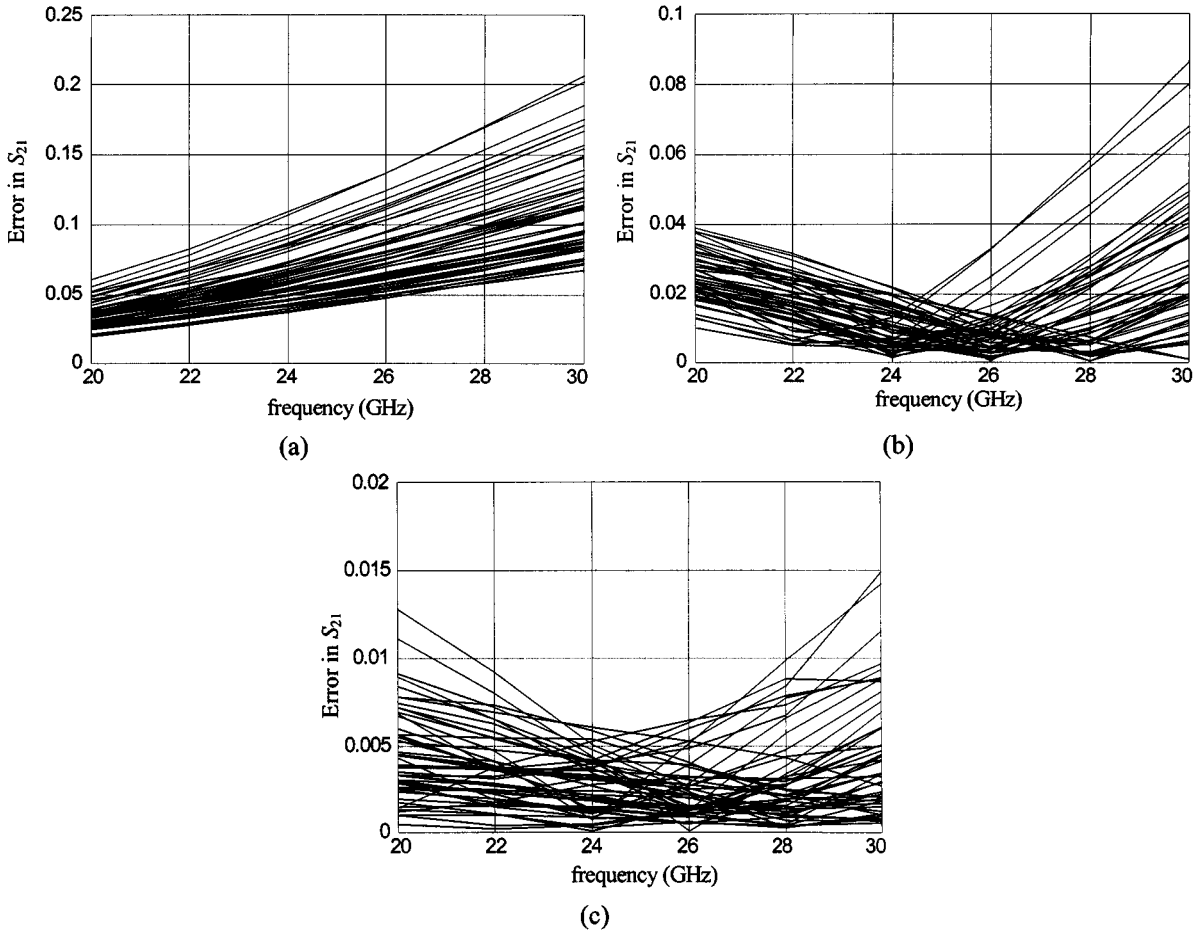

Fig. 8. Error in S_{21} with respect to em by: (a) the microstrip transmission-line model, (b) the microstrip transmission-line SMSM, and (c) the microstrip transmission-line FSMSM.

TABLE I
REGION OF INTEREST FOR THE MICROSTRIP-LINE EXAMPLE

Parameter	Minimum value	Maximum value
W	10 mil	30 mil
L	40 mil	60 mil
H	10 mil	20 mil
ε_r	8	10

in Table I. The frequency range is 20–30 GHz with a step of 2 GHz ($F_p = 6$). The characteristic impedance Z_0 of the transmission line is computed in terms of the width W_c, the substrate height H_c, and the relative dielectric constant ε_{rc} using the quasi-static model in [7]. Only nine points ($B_p = 9$) in the region of interest were used to develop SMSM or FSMSM. We developed SMSM and FSMSM for the microstrip line, and the corresponding mapping parameters for each case are given in Table II. Notice that, in case of SMSM, the mapping parameters $\boldsymbol{s}$, δ, $\boldsymbol{t}$, σ are fixed, and in the case of FSMSM, the computed value of $\boldsymbol{t}$ is $\mathbf{0}$, which means that the coarse-model frequency does not depend on the fine-model parameters (it only depends on the fine-model frequency). The microstrip transmission-line SMSM and FSMSM were tested at 50 uniformly distributed random points in the region of interest. The

TABLE II
SMSM AND FSMSM MAPPING PARAMETERS FOR THE MICROSTRIP TRANSMISSION LINE

	SMSM	FSMSM
$\boldsymbol{B}$	$\begin{bmatrix} 1.015 & -0.002 & -0.007 & -0.022 \\ -0.001 & 0.992 & 0.020 & 0.023 \\ -0.008 & 0.001 & 0.985 & 0.027 \\ 0.009 & -0.004 & 0.044 & 1.028 \end{bmatrix}$	$\begin{bmatrix} 1.026 & -0.005 & 0.006 & -0.021 \\ -0.009 & 0.965 & -0.011 & 0.017 \\ -0.002 & 0.004 & 0.979 & 0.022 \\ 0.019 & -0.001 & 0.020 & 1.025 \end{bmatrix}$
$\boldsymbol{c}$	$[-0.011 \quad -0.008 \quad 0.012 \quad -0.036]^T$	$[-0.013 \quad 0.001 \quad 0.011 \quad -0.010]^T$
$\boldsymbol{s}$	$\mathbf{0}$ (fixed)	$[-0.006 \quad 0 \quad 0.002 \quad -0.002]^T$
$\boldsymbol{t}$	$\mathbf{0}$ (fixed)	$\mathbf{0}$
σ	1 (fixed)	1.035
δ	0 (fixed)	0.001

error in S_{21} defined by (13) for the microstrip transmission-line model is shown in Fig. 8(a). Fig. 8(b) and (c) show the error in S_{21} by the microstrip transmission-line SMSM and by the microstrip transmission-line FSMSM, respectively. The error of the microstrip transmission-line FSMSM is approximately four times less than the corresponding error of the microstrip transmission-line SMSM. The time taken by the EM solver

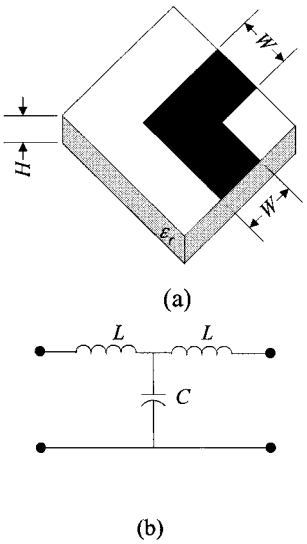

Fig. 9. Microstrip right-angle bend. (a) Fine model. (b) Coarse model.

TABLE III
REGION OF INTEREST FOR THE MICROSTRIP RIGHT-ANGLE BEND

Parameter	Minimum value	Maximum value
W	20 mil	30 mil
H	8 mil	16 mil
ε_r	8	10

and the Huber optimizer is 90 and 30 s, respectively, on an HP C200-RISC workstation.

B. Microstrip Right-Angle Bend

In this example, we compare between two coarse models for the microstrip right-angle bend. The first coarse model is taken from [8] and is referred to as Gupta's model. The second coarse model is taken from [9] and is referred to as Jansen's model. Both coarse models provide empirical formulas for the *LC* circuit in Fig. 9. The fine model is analyzed by Sonnet Software's ***em***, as shown in Fig. 9(a). The fine- and coarse-model parameters are given by $\boldsymbol{x}_f = [W \;\; H \;\; \varepsilon_r]^T$, $\boldsymbol{x}_c = [W_c \;\; H_c \;\; \varepsilon_{rc}]^T$. The region of interest is given in Table III. The frequency range is 1–31 GHz with a step of 2 GHz ($F_p = 16$). The number of base points in the region of interest is seven ($B_p = 7$).

The FSMSM was developed for the two coarse models, and the corresponding mapping parameters are given in Table IV. The enhanced Gupta's and Jansen's models were tested at 50 random points in the region of interest. The error in S_{11} by the Gupta's and Jansen's models is shown in Fig. 10. The error in S_{11} by the enhanced Gupta's and Jansen's models is shown in Fig. 11.

It is difficult to compare between the two coarse models since Jansen's model is more accurate at lower frequencies (see Fig. 10) and Gupta's model is slightly more accurate at higher frequencies. However, after developing FSMSM for each coarse model, we can compare between the two coarse models according to the criteria in Section II. The values of β given by (9) for the enhanced Gupta's and Jansen's models are 3.4 and 3.5, respectively. We notice that the value of β in both cases is approximately the same, which means that the accuracy of both coarse models with respect to the fine model is comparable. The time taken by the EM solver and Huber optimizer is 6 min and 40 s, respectively, on an HP C200-RISC workstation.

TABLE IV
FSMSM MAPPING PARAMETERS FOR THE MICROSTRIP RIGHT-ANGLE BEND

	Gupta's model [8]	Jansen's model [9]
$\boldsymbol{B}$	$\begin{bmatrix} 1.291 & 0.207 & 0.189 \\ 0.067 & 0.613 & -0.094 \\ 0.092 & -0.066 & 0.918 \end{bmatrix}$	$\begin{bmatrix} 2.768 & 0.314 & 0.276 \\ -0.042 & 1.282 & 0.318 \\ -0.018 & -0.013 & 0.421 \end{bmatrix}$
$\boldsymbol{c}$	$[0.094 \;\; -0.174 \;\; 0.123]^T$	$[0.048 \;\; -0.012 \;\; 0.031]^T$
$\boldsymbol{s}$	$[0.109 \;\; -0.296 \;\; 0.183]^T$	$[0.001 \;\; -0.053 \;\; 0.250]^T$
$\boldsymbol{t}$	$[-0.001 \;\; -0.002 \;\; -0.002]^T$	$[-0.001 \;\; -0.002 \;\; -0.001]^T$
σ	3.269	2.343
δ	0.019	0.015

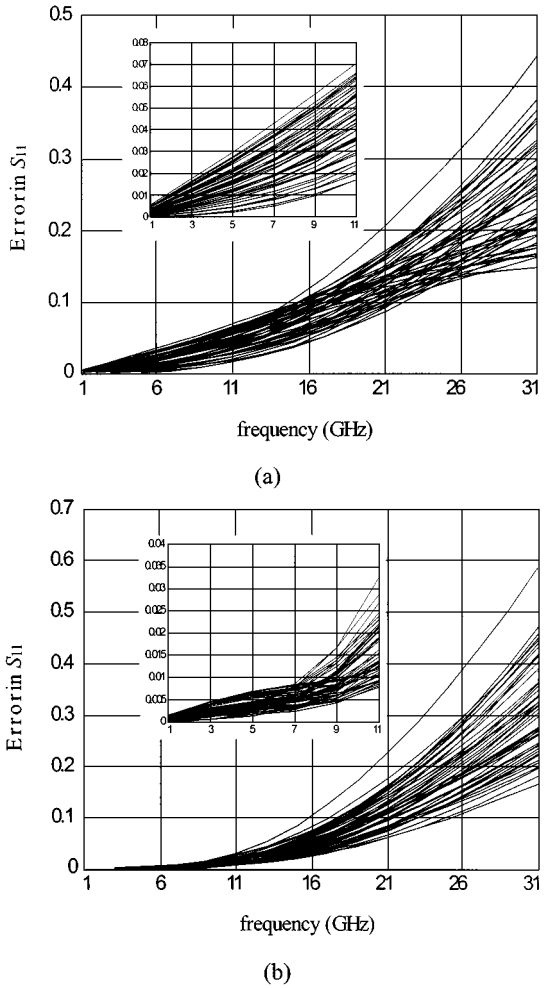

Fig. 10. Error in S_{11} of the microstrip right-angle bend with respect to ***em*** by: (a) Gupta's model [8] and (b) Jansen's model [9].

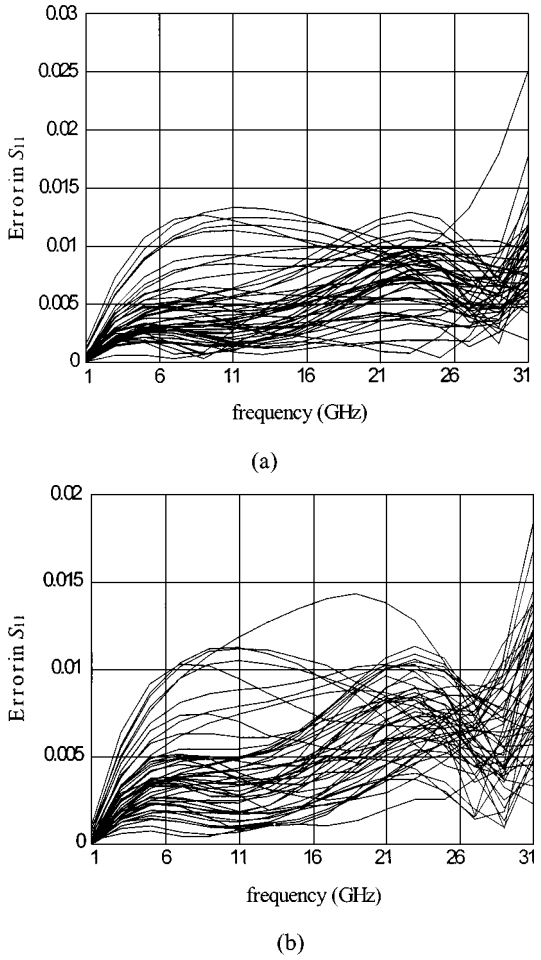

Fig. 11. Error in S_{11} of the microstrip right-angle bend with respect to ***em*** by: (a) the enhanced Gupta's model [8] and (b) the enhanced Jansen's model [9].

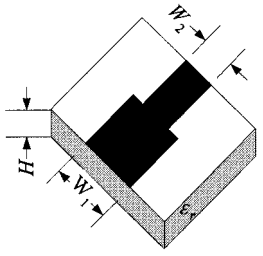

Fig. 12. Microstrip step junction.

C. Microstrip Step Junction

In this example we demonstrate the MSMDR. The fine model of the microstrip step junction (Fig. 12) is analyzed by Sonnet Software's ***em***. The coarse model is a built-in element of OSA90/hope. The fine- and coarse-model parameters are given by $\boldsymbol{x}_f = [W_1 \quad W_2 \quad H \quad \varepsilon_r]^T, \boldsymbol{x}_c = [W_{1c} \quad W_{2c} \quad H_c \quad \varepsilon_{rc}]^T$. The region of interest is given in Table V. The frequency range is 2–40 GHz with a step of 2 GHz ($F_p = 20$). The number of base points in the region of interest is nine ($B_p = 9$). There are six responses to be matched: the real and imaginary parts of S_{11}, S_{21}, and S_{22}. We will show that one mapping targeting all these responses is not sufficient to achieve the required accuracy at the base points.

TABLE V
REGION OF INTEREST FOR THE MICROSTRIP STEP JUNCTION

Parameter	Minimum value	Maximum value
W_1	20 mil	40 mil
W_2	10 mil	20 mil
H	10 mil	20 mil
ε_r	8	10

TABLE VI
MSMDR MAPPING PARAMETERS FOR THE MICROSTRIP STEP JUNCTION

	Target responses are {Im[S_{11}], Im[S_{21}], Im[S_{22}], Re[S_{21}]}	Target responses are {Re[S_{11}], Re[S_{22}]}
$\boldsymbol{B}$	$\begin{bmatrix} 0.764 & 0.033 & -0.062 & 0.074 \\ 0.191 & 0.632 & 0.255 & -0.502 \\ -0.023 & 0.116 & 1.485 & 0.018 \\ 0.676 & -0.365 & -0.111 & 0.177 \end{bmatrix}$	$\begin{bmatrix} 3.071 & -0.008 & -0.010 & -0.004 \\ 0.008 & 0.202 & 0.032 & 0.004 \\ -0.001 & 0.001 & 1.152 & 0.000 \\ -0.077 & -0.118 & -0.002 & 1.241 \end{bmatrix}$
$\boldsymbol{c}$	$[0.002 \quad -0.002 \quad 0.002 \quad -0.006]^T$	$[-0.001 \quad 0.001 \quad 0.000 \quad -0.003]^T$
$\boldsymbol{s}$	$[-0.003 \quad 0.004 \quad -0.001 \quad -0.002]^T$	$\boldsymbol{0}$
$\boldsymbol{t}$	$[-0.001 \quad 0.000 \quad -0.005 \quad 0.000]^T$	$[-0.001 \quad 0.000 \quad -0.007 \quad 0.003]^T$
σ	1.546	5.729
δ	0.113	0.065

TABLE VII
REGION OF INTEREST FOR THE MICROSTRIP-SHAPED T-JUNCTION

Parameter	Minimum value	Maximum value
h	15 mil	25 mil
x	5 mil	15 mil
y	5 mil	15 mil
ε_r	8	10

The required accuracy is $E_{ij} \leq 0.03$, $i = 1, 2$ and $j = 1, 2$ where E_{ij} is defined by (13). Fig. 13(a) shows the error in S_{11} before applying any modeling technique, while Fig. 13(b) shows it after developing a single mapping for all responses. The results obtained by a single mapping do not satisfy the required accuracy.

The MSMDR algorithm (in Section III) was applied to align the two models. The algorithm divided the responses into two groups $\{\mathrm{Im}[S_{11}], \mathrm{Im}[S_{21}], \mathrm{Im}[S_{22}], \mathrm{Re}[S_{21}]\}$, and $\mathrm{Re}[S_{11}]$, $\mathrm{Re}[S_{22}]\}$ and developed a separate mapping for each group of responses. The corresponding mapping parameters for each group are given in Table VI. Fig. 13(c) shows the error in S_{11} at the base points after applying the MSMDR algorithm. We notice that the specified accuracy is achieved.

The enhanced coarse model of the step junction was tested at 50 uniformly distributed random points. The errors in S_{11} and S_{21} by the coarse model are shown in Fig. 14(a) and (b), respectively. The errors in S_{11} and S_{21} by the enhanced coarse model are shown in Fig. 15(a) and (b), respectively. The histograms of the error in S_{21} at 40 GHz (which is the maximum error in the frequency range 2–40 GHz) by the coarse model and by the enhanced coarse model are shown in Fig. 16(a) and (b), respectively. The mean and standard deviation for the two cases

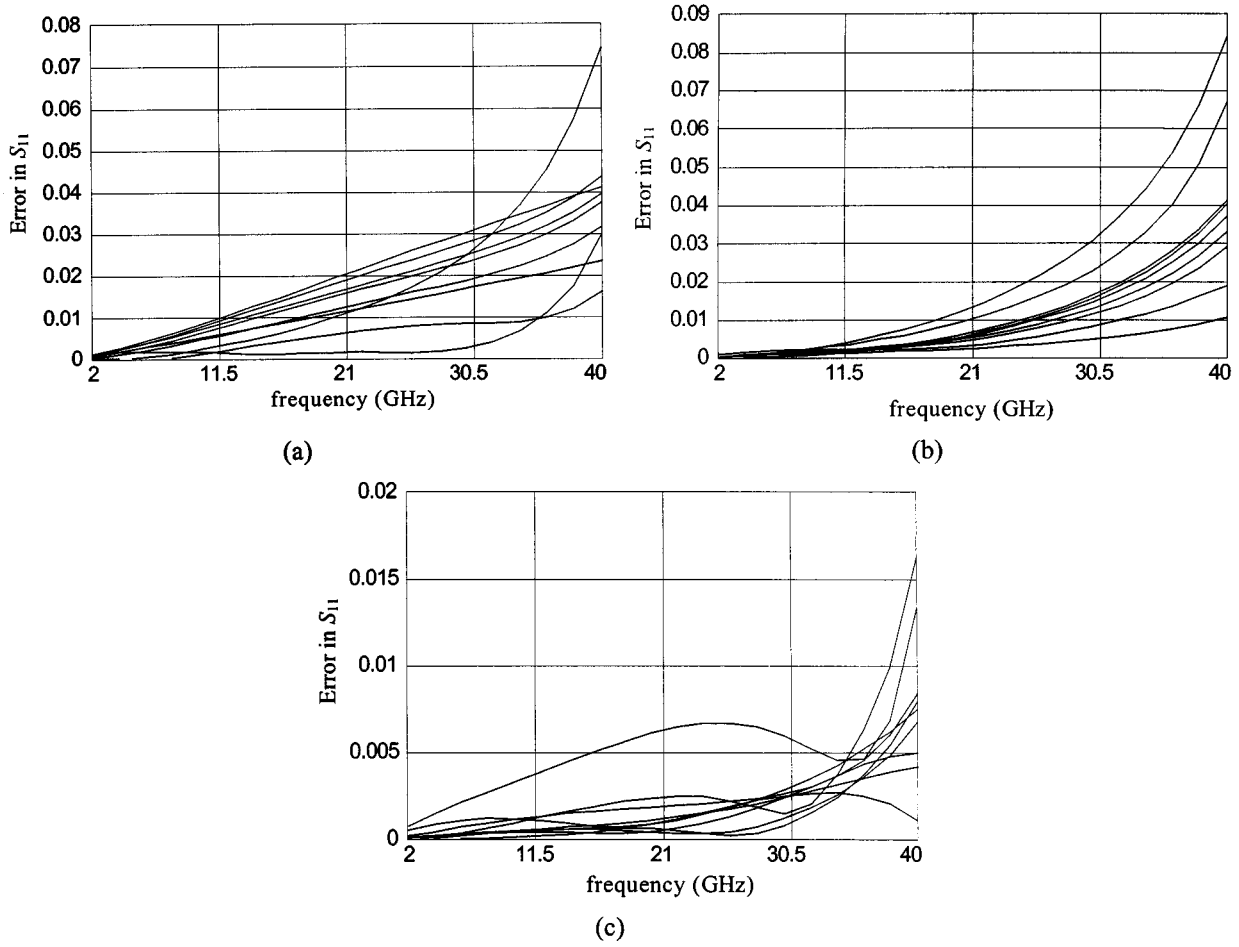

Fig. 13. Error in S_{11} of the microstrip step junction with respect to ***em***: (a) before applying any modeling technique, (b) after applying FSMSM, and (c) after applying the MSMDR algorithm.

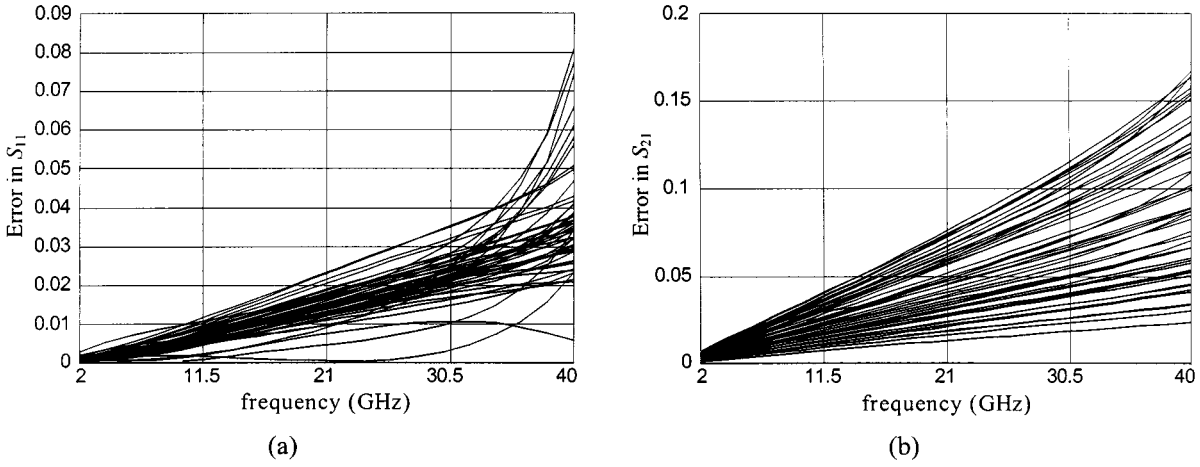

Fig. 14. Error of the microstrip step-junction coarse model with respect to ***em*** in: (a) S_{11} and (b) S_{21}.

are also shown in Fig. 16(a) and (b). The time taken by the EM solver and by the Huber optimizer is 19 and 2.5 min, respectively, on an HP C200-RISC workstation.

D. Microstrip-Shaped T-Junction

In this example, we consider a shaped T-junction [see Fig. 17(a)]. This T-junction was introduced in [10] to compensate discontinuities. It was recently compared in [11] with the other T-junction configurations in the literature. The T-junction is symmetric in the sense that all input lines have the same width w. The fine model is analyzed by Sonnet Software's ***em*** and the coarse model is composed of empirical models of simple microstrip elements [see Fig. 17(b)] of OSA90/hope. The fine- and coarse-model parameters

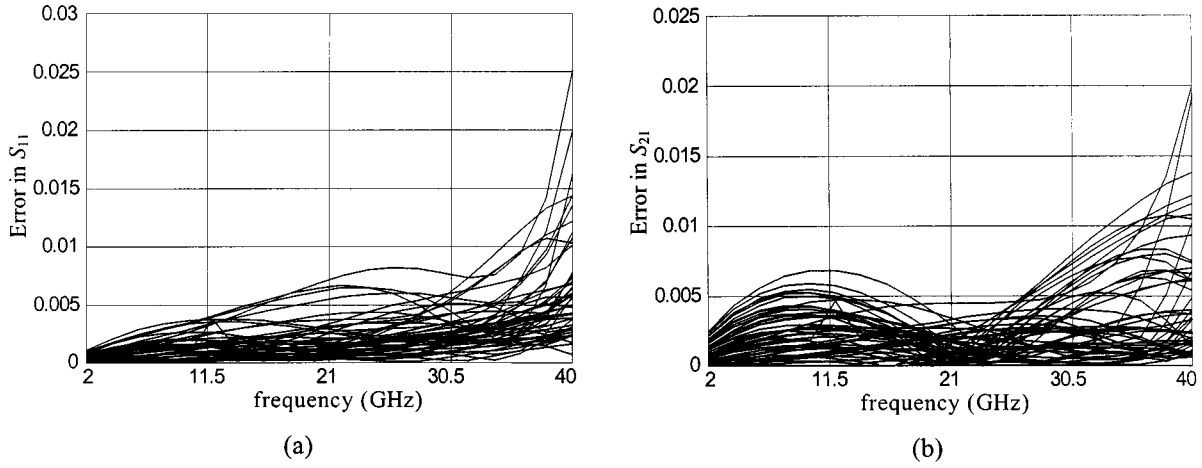

Fig. 15. Error of the microstrip step-junction enhanced coarse model with respect to ***em*** in: (a) S_{11} and (b) S_{21}.

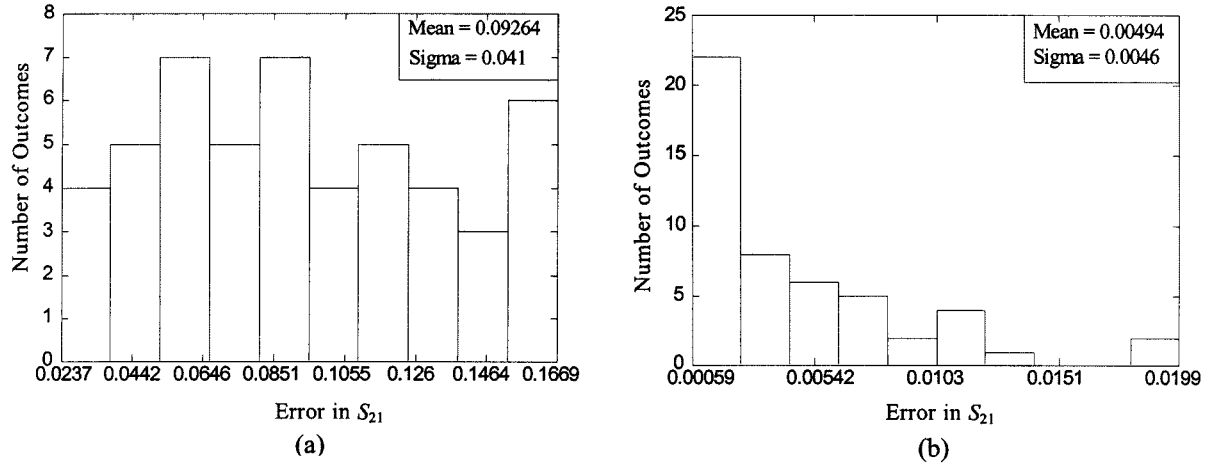

Fig. 16. Histogram of the error in S_{21} of the microstrip step junction for 50 points in the region of interest at 40 GHz by: (a) the coarse model and (b) enhanced coarse model.

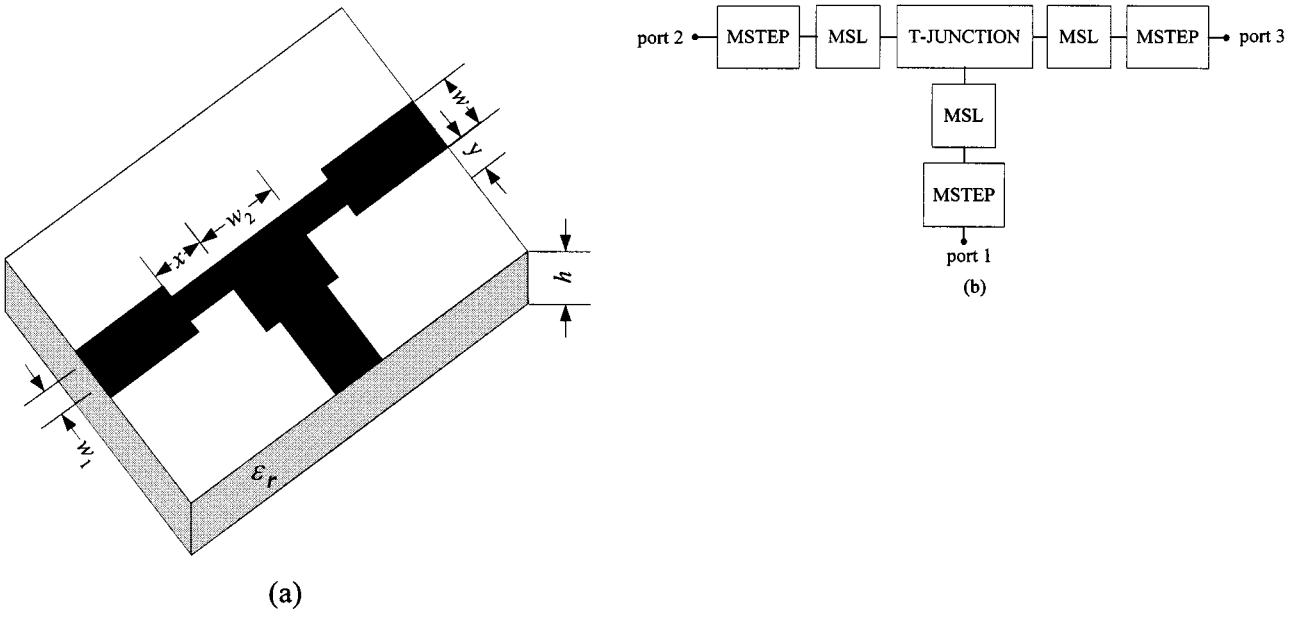

Fig. 17. Microstrip-shaped T-junction. (a) The physical structure (fine model). (b) The coarse model.

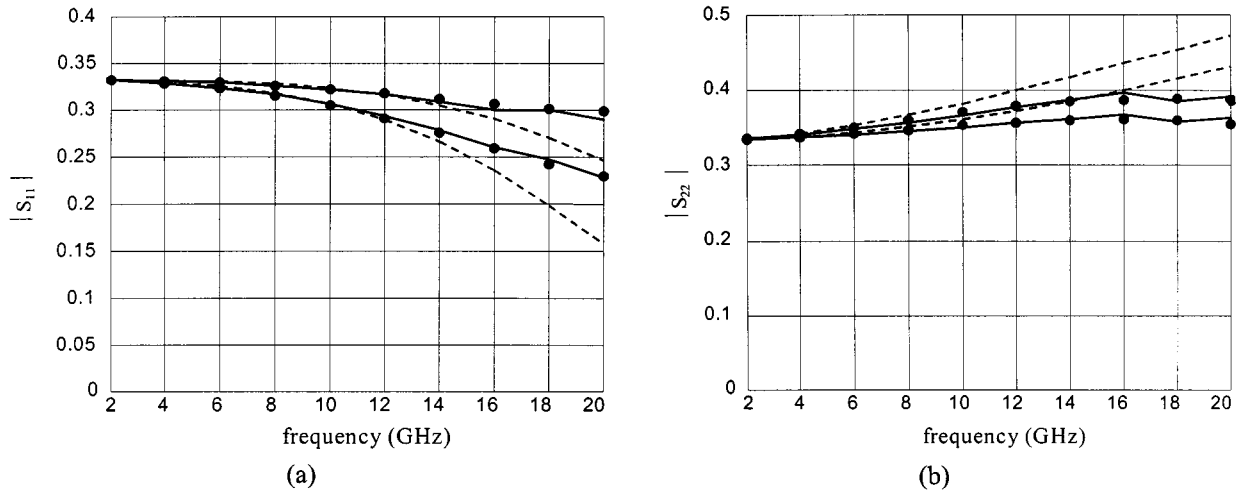

Fig. 18. Responses of the shaped T-Junction at two test points in the region of interest by Sonnet Software's *em* (•) by the coarse model (—) and by the enhanced coarse model (—). (a) $|S_{11}|$. (b) $|S_{22}|$.

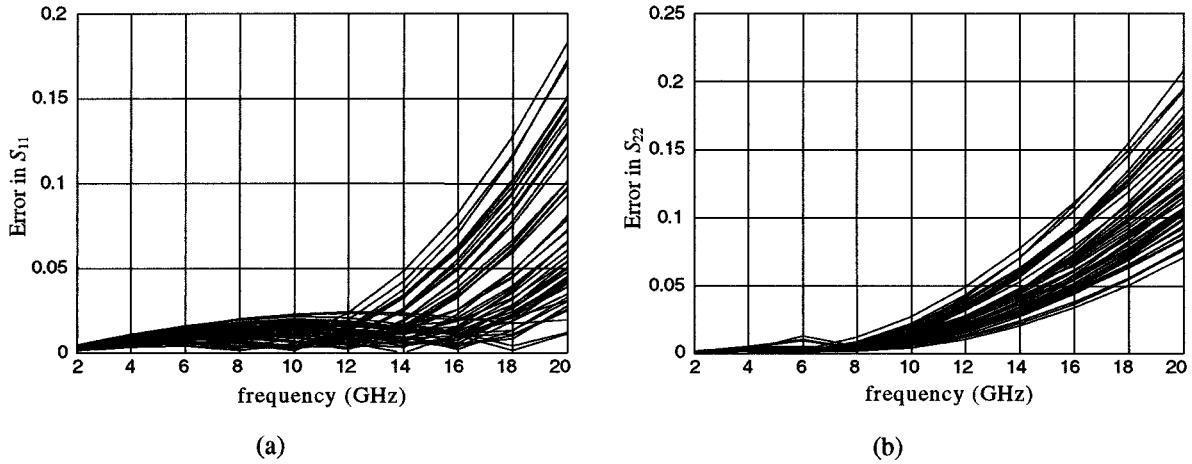

Fig. 19. Error of the shaped T-junction coarse model with respect to ***em*** in: (a) S_{11} and (b) S_{22}.

are given by $\boldsymbol{x}_f = [w \quad h \quad w_1 \quad w_2 \quad x \quad y \quad \varepsilon_r]^T$, $\boldsymbol{x}_c = [w_c \quad h_c \quad w_{1c} \quad w_{2c} \quad x_c \quad y_c \quad \varepsilon_{cr}]^T$.

The region of interest is given in Table VII and the frequency range used is 2–20 GHz with a step of 2 GHz ($F_p = 10$). The width w of the input lines is determined in terms of h and ε_r so that the characteristic impedance of the input lines is 50 Ω. The width w_1 is taken as 1/3 of the width w. The width w_2 is obtained so that the characteristic impedance of the microstrip line after the step connected to port 2 is twice the characteristic impedance of the microstrip line after the step connected to port 1 [see Fig. 17(b)]. The number of base points in the region of interest is 9 ($B_p = 9$).

The MSMFI algorithm (in Section III) was applied to enhance the accuracy of the T-Junction coarse model. The algorithm divided the total frequency range into two intervals: 2–16 GHz and 16–20 GHz. The corresponding mapping parameters for each interval are given in Table VIII. Fig. 18(a) and (b) shows $|S_{11}|$ and $|S_{22}|$ by Sonnet Software's ***em***, the T-junction coarse model and the T-junction enhanced coarse model at two test points in the region of interest. To perform a more comprehensive test, 50 random points were generated in the region of interest. The coarse-model errors in S_{11} and S_{22} defined by (13) are shown in Fig. 19(a) and (b), respectively. The enhanced coarse-model errors in S_{11} and S_{22} are shown in Fig. 20(a) and (b), respectively. The time taken by the EM solver and by the Huber optimizer is 11 and 23 min, respectively, on an HP C200-RISC workstation.

The enhanced coarse model for the shaped T-Junction can be utilized in optimization. For example, the T-junction is optimized here to achieve the minimum possible mismatch at the three ports. The optimization variables are x and y, the other parameters are kept fixed ($w = 24$ mil, $h = 25$ mil, and $\varepsilon_r = 9.9$) [11]. The specifications [11] are $|S_{11}| \leq 1/3$, $|S_{22}| \leq 1/3$ in the frequency range of 2 –16 GHz. The minimax optimizer in OSA90/hope reached the solution $x = 2.1$ mil and $y = 21.1$ mil, which agrees with the solution obtained in [11]. The magnitude of S_{11} and S_{22} obtained by Sonnet Software's ***em***, the coarse model and the enhanced coarse model are shown in Fig. 21(a) and (b). We notice a good agreement between the results obtained by the enhanced coarse model and by Sonnet Software's ***em***.

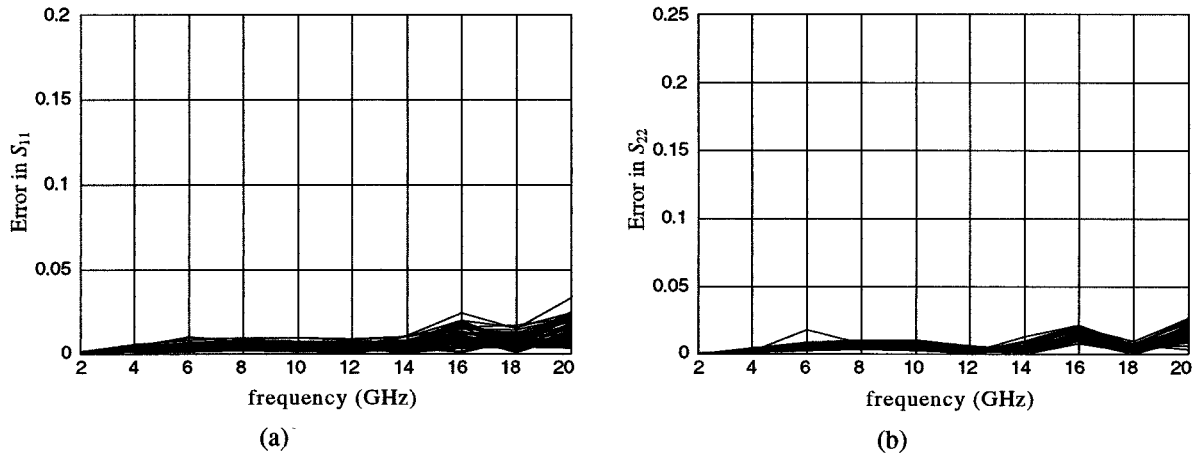

Fig. 20. Error of the shaped T-junction enhanced coarse model with respect to ***em*** in: (a) S_{11} and (b) S_{22}.

TABLE VIII
MSMFI MAPPING PARAMETERS FOR THE MICROSTRIP SHAPED T-JUNCTION

	2 GHz to 16 GHz	16 GHz to 20 GHz
$\boldsymbol{B}$	$\begin{bmatrix} 1.04 & 0.07 & 0.01 & 0.08 & -0.06 & 0.00 & 0.22 \\ 0.00 & 0.89 & 0.00 & -0.07 & -0.20 & 0.06 & -0.03 \\ -0.00 & 0.07 & 0.99 & 0.04 & -0.12 & 0.01 & -0.06 \\ -0.04 & 0.00 & -0.01 & 0.97 & 0.10 & -0.06 & -0.27 \\ 0.01 & 0.04 & 0.00 & 0.03 & 0.99 & -0.05 & -0.03 \\ -0.13 & -0.05 & -0.04 & -0.16 & 0.12 & 0.99 & 0.62 \\ -0.08 & 0.12 & -0.03 & 0.00 & -0.07 & 0.03 & 0.83 \end{bmatrix}$	$\begin{bmatrix} 0.99 & 0.02 & -0.00 & 0.01 & -0.09 & -0.01 & 0.13 \\ 0.05 & 0.85 & 0.01 & -0.07 & -0.28 & 0.01 & -0.01 \\ -0.06 & 0.15 & 0.98 & 0.04 & -0.25 & 0.00 & 0.02 \\ -0.10 & -0.06 & -0.03 & 0.88 & 0.13 & -0.09 & -0.27 \\ 0.08 & 0.04 & 0.03 & 0.11 & 1.07 & -0.04 & -0.12 \\ -0.14 & -0.02 & -0.05 & -0.15 & 0.23 & 1.03 & 0.51 \\ -0.13 & 0.22 & -0.04 & 0.02 & -0.07 & 0.03 & 0.87 \end{bmatrix}$
$\boldsymbol{c}$	$[0.02 \quad 0.01 \quad -0.01 \quad -0.03 \quad -0.01 \quad 0.07 \quad -0.03]^T$	$[0.01 \quad 0.01 \quad -0.01 \quad -0.03 \quad -0.01 \quad 0.05 \quad -0.03]^T$
$\boldsymbol{s}$	$[-0.01 \quad 0.09 \quad -0.10 \quad -0.02 \quad 0.00 \quad -0.02 \quad -0.20]^T$	$[0.00 \quad 0.01 \quad -0.01 \quad 0.00 \quad 0.00 \quad 0.00 \quad -0.02]^T$
$\boldsymbol{t}$	$\boldsymbol{0}$	$[0.01 \quad 0.00 \quad -0.02 \quad 0.00 \quad 0.00 \quad 0.00 \quad 0.00]^T$
σ	0.851	0.957
δ	−0.003	0.008

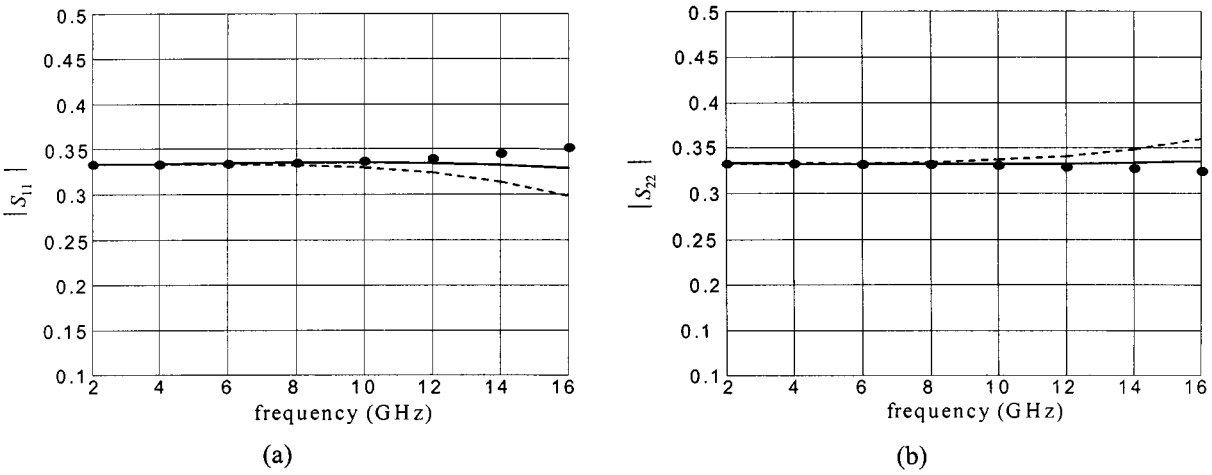

Fig. 21. Responses of the optimum shaped T-Junction by Sonnet Software's ***em*** (•) by the coarse model (—) and enhanced coarse model (—). (a) $|S_{11}|$. (b) $|S_{22}|$.

VI. Conclusions

The powerful GSM approach to microwave device modeling has been introduced in this paper. Three derivative concepts have been illustrated: the SMSM concept, FSMSM concept, and MSM concept. Two variations of MSM are also presented: MSMDR and MSMFI. Our approach typically uses only a few EM simulations to dramatically enhance the accuracy of existing empirical device models. It involves only simple matrix operations, which makes it an effective computer-aided design (CAD) tool in terms of CPU time, memory requirement, ease of use, and accuracy. It also preserves the compactness and simplicity of the original empirical models. Three software tools are required to implement GSM: an optimizer (the Huber optimizer is recommended since it is robust against large errors in the data), a suitable circuit simulator, and a suitable full-wave EM simulator.

Acknowledgment

The authors would like to thank former colleagues Dr. R. M. Biernacki, Agilent EEsof EDA, Santa Rosa, CA, and Dr. S. H. Chen, Agilent EEsof EDA, Santa Rosa, CA, for useful discussions on the SMSM concept at an early stage of its development. The authors would also like to thank Dr. J. C. Rautio, Sonnet Software Inc., Liverpool, NY, for making *em* available.

References

[1] J. W. Bandler, R. M. Biernacki, S. H. Chen, P. A. Grobelny, and R. H. Hemmers, "Space mapping technique for electromagnetic optimization," *IEEE Trans. Microwave Theory Tech.*, vol. 42, pp. 2536–2544, Dec. 1994.

[2] J. W. Bandler, R. M. Biernacki, S. H. Chen, R. H. Hemmers, and K. Madsen, "Electromagnetic optimization exploiting aggressive space mapping," *IEEE Trans. Microwave Theory Tech.*, vol. 43, pp. 2874–2882, Dec. 1995.

[3] J. W. Bandler, R. M. Biernacki, S. H. Chen, and Q. H. Wang, "Multiple space mapping EM optimization of signal integrity in high-speed digital circuits," in *Proc. 5th Int. Integrated Nonlinear Microwave Millimeter-Wave Circuits Workshop*, Duisburg, Germany, 1998, pp. 138–140.

[4] J. W. Bandler, S. H. Chen, R. M. Biernacki, L. Gao, K. Madsen, and H. Yu, "Huber optimization of circuits: A robust approach," *IEEE Trans. Microwave Theory Tech.*, vol. 41, pp. 2279–2287, Dec. 1993.

[5] R. M. Biernacki, J. W. Bandler, J. Song, and Q. J. Zhang, "Efficient quadratic approximation for statistical design," *IEEE Trans. Circuit Syst.*, vol. 36, pp. 1449–1454, Nov. 1989.

[6] J. W. Bandler, R. M. Biernacki, and S. H. Chen, "Parameterization of arbitrary geometrical structures for automated electromagnetic optimization," in *IEEE MTT-S Int. Microwave Symp. Dig.*, San Francisco, CA, 1996, pp. 1059–1062.

[7] D. M. Pozar, *Microwave Engineering*. Reading, MA: Addison-Wesley, 1990.

[8] K. C. Gupta, R. Garg, and I. J. Bahl, *Microstrip Lines and Slotlines*. Norwood, MA: Artech House, 1979.

[9] M. Kirschning, R. Jansen, and N. Koster, "Measurement and computer-aided modeling of microstrip discontinuities by an improved resonator method," in *IEEE MTT-S Int. Microwave Symp. Dig.*, Boston, MA, 1983, pp. 495–497.

[10] M. Dydyk, "Master the T-junction and sharpen your MIC designs," *Microwaves*, pp. 184–186, 1977.

[11] J. W. Bandler, M. H. Bakr, N. Georgieva, M. A. Ismail, and D. G. Swanson, Jr., "Recent results in electromagnetic optimization of microwave components including microstrip T-junction," in *Appl. Comput. Electromag. Soc. Conf.*, Monterey, CA, 1999, pp. 326–333.

John W. Bandler (S'66–M'66–SM'74–F'78) was born in Jerusalem, on November 9, 1941. He studied at the Imperial College of Science and Technology, London, U.K., from 1960 to 1966. He received the B.Sc. (Eng.), Ph.D., and D.Sc. (Eng.) degrees from the University of London, London, U.K., in 1963, 1967, and 1976, respectively.

In 1966, he joined Mullard Research Laboratories, Redhill, Surrey, U.K. From 1967 to 1969, he was a Post-Doctorate Fellow and Sessional Lecturer at the University of Manitoba, Winnipeg, MB, Canada. In 1969, he joined McMaster University, Hamilton, ON, Canada, where he has served as Chairman of the Department of Electrical Engineering and Dean of the Faculty of Engineering. He is currently a Professor Emeritus in Electrical and Computer Engineering, and directs research in the Simulation Optimization Systems Research Laboratory. He is a member of the Micronet Network of Centres of Excellence. He was President of Optimization Systems Associates Inc. (OSA), which he founded in 1983, until November 20, 1997, the date of acquisition of OSA by Hewlett-Packard Company (HP). OSA implemented a first-generation yield-driven microwave computer-aided design (CAD) capability for Raytheon in 1985, followed by further innovations in linear and nonlinear microwave CAD technology for the Raytheon/Texas Instruments Incorporated Joint Venture MIMIC Program. OSA introduced the computer-aided engineering (CAE) systems RoMPE in 1988, HarPE in 1989, OSA90 and OSA90/hope in 1991, Empipe in 1992, and Empipe3D and EmpipeExpress in 1996. OSA created the product ***empath*** in 1996, which was marketed by Sonnet Software Inc., Liverpool, NY. He is President of the Bandler Corporation, Dundas, ON, Canada, which he founded in 1997. He has authored or co–authored over 320 papers from 1965 to 2000. He contributed to *Modern Filter Theory and Design* (New York: Wiley, 1973) and to *Analog Methods for Computer-aided Analysis and Diagnosis* (New York: Marcel Dekker, 1988). Four of his papers have been reprinted in *Computer-Aided Filter Design* (New York: IEEE Press, 1973), one in each of *Microwave Integrated Circuits* (Norwood, MA: Artech House, 1975), *Low-Noise Microwave Transistors and Amplifiers* (New York: IEEE Press, 1981), *Microwave Integrated Circuits, 2nd ed.* (Norwood, MA: Artech House, 1985), *Statistical Design of Integrated Circuits* (New York: IEEE Press, 1987), and *Analog Fault Diagnosis* (New York: IEEE Press, 1987). He joined the Editorial Boards of the *International Journal of Numerical Modeling* in 1987, the *International Journal of Microwave and Millimeterwave Computer-Aided Engineering* in 1989, and *Optimization and Engineering* in 1998. He was guest editor of the *International Journal of Microwave and Millimeter-Wave Computer-Aided Engineering* "Special Issue on Optimization-Oriented Microwave CAD" (1997).

Dr. Bandler is a Fellow of the Royal Society of Canada, a Fellow of the Institution of Electrical Engineers (IEE), U.K., a Fellow of the Engineering Institute of Canada, a member of the Association of Professional Engineers of the Province of Ontario (Canada), and a member of the Massachusetts Institute of Technology (MIT) Electromagnetics Academy. He was an associate editor of the IEEE TRANSACTIONS ON MICROWAVE THEORY AND TECHNIQUES (1969–1974), and has continued serving as a member of the Editorial Board. He was guest editor of the Special Issue on "Computer-Oriented Microwave Practices" of the IEEE TRANSACTIONS ON MICROWAVE THEORY AND TECHNIQUES (1974), guest co-editor of the Special Issue on "Process-Oriented Microwave CAD and Modeling" of the IEEE TRANSACTIONS ON MICROWAVE THEORY AND TECHNIQUES (1992), and guest editor of the Special Issue on "Automated Circuit Design Using Electromagnetic Simulators" of the TRANSACTIONS ON MICROWAVE THEORY AND TECHNIQUES (1997). He is currently co-chair of the MTT-1 Technical Committee on Computer-Aided Design. He was the recipient of the 1994 Automatic Radio Frequency Techniques Group (ARFTG) Automated Measurements Career Award.

Natalia Georgieva (S'93–M'97) received the Dipl. Eng. degree from the Technical University of Varna, Varna, Bulgaria, in 1989, and the Doctor of Engineering degree from the University of Electro-Communications, Tokyo, Japan, in 1997.

In July 1999, she joined the Department of Electrical and Computer Engineering, McMaster University, Hamilton, ON, Canada, where she is currently an Assistant Professor. Her research was carried out in the Simulation Optimizations Systems Research Laboratory, McMaster University. Her research interests include computational electromagnetics, analysis and modeling of high-frequency structures, as well as CAD tools for microwave/millimeter-wave devices and antennas.

Dr. Georgieva held the 1998–1999 Natural Sciences and Engineering Research Council (NSERC) of Canada Post-Doctoral Fellowship. She was the recipient of the 2000 NSERC University Faculty Award.

Mostafa A. Ismail (S'98) was born in Cairo, Egypt, on May 21, 1968. He received the B.Sc. degree in electronics and communications engineering and the Masters degree in engineering mathematics from Cairo University, Cairo, Egypt, in 1991 and 1995, respectively, and is currently working toward the Ph.D. degree at McMaster University, Hamilton, ON, Canada.

In October 1991, he joined the Department of Engineering Mathematics and Physics, Faculty of Engineering, Cairo University. In September 1997, he joined the Department of Electrical and Computer Engineering, McMaster University, where his research is carried out in the Simulation Optimization Systems Research Laboratory. His research interests are computer-aided design and modeling of microwave circuits.

Mr. Ismail was the recipient of a one-year Nortel Networks Ontario Graduate Scholarship in Science and Technology in 2000.

José E. Rayas-Sánchez (S'88–M'89–SM'95) was born in Guadalajara, Jalisco, Mexico, on December 27, 1961. He received the B.Sc. degree in electronics engineering from the Instituto Tecnológico y de Estudios Superiores de Occidente (ITESO), Guadalajara, Mexico, in 1984, the Masters degree in electrical engineering at the Instituto Tecnológico y de Estudios Superiores de Monterrey (ITESM), Monterrey, Mexico, in 1989, and is currently working toward the Ph.D. degree in electrical engineering at McMaster University, Hamilton, ON, Canada.

From 1989 to 1997, he was a Full-Time Professor in the Electrical and Computer Engineering Department, ITESO. He joined the Simulation Optimization Systems Research Laboratory, McMaster University, in 1997. His research focuses on the development of novel methods and techniques for computer-aided modeling, design, and optimization of analog wireless electronic circuits and devices exploiting SM and ANNs.

Mr. Rayas-Sánchez was the recipient of a 1997–2000 Consejo Nacional de Ciencia y Tecnología (CONACYT) Scholarship presented by the Mexican Government, as well as a 2000–2001 Ontario Graduate Scholarship presented by the Ministry of Training for Colleges and Universities in Ontario.

Qi-Jun Zhang (M'87-SM'95) received the B.Eng. degree from East China Engineering Institute, Nanjing, China, in 1982, and the Ph.D. degree in electrical engineering from McMaster University, Hamilton, ON, Canada, in 1987.

In 1982 and 1983, he was with the System Engineering Institute, Tianjin University, Tianjin, China. From 1988 to 1990, he was with Optimization Systems Associates Inc. (OSA), Dundas, ON, Canada, where he developed advanced microwave optimization software. In 1990, he joined the Department of Electronics, Carleton University, Ottawa, ON, Canada, where he is currently a Professor. His research interests are neural-network and optimization methods for high-speed/high-frequency circuit design. He has authored *Neural Networks for RF and Microwave Design* (Norwood, MA: Artech House, 2000), co-edited *Modeling and Simulation of High-Speed VLSI Interconnects* (Norwell, MA: Kluwer), and contributed to *Analog Methods for Computer-Aided Analysis and Diagnosis* (New York: Marcel Dekker, 1988). He was a Guest Co-Editor for the Special Issue on "High-Speed VLSI Interconnects" for the *International Journal of Analog Integrated Circuits and Signal Processing* (Norwell, MA: Kluwer, 1994), a Guest Editor for the first Special Issues on "Applications of ANN to RF and Microwave Design" for the *International Journal of RF and Microwave Computer-Aided Engineering* (New York: Wiley, 1999), and a Guest Editor for the second Special Issues on "Applications of ANN to RF and Microwave Design" for the *International Journal of RF and Microwave CAE* (New York: Wiley, to be published in 2001).

Dr. Zhang is a member of the Association of Professional Engineers Ontario.